Supplementary Information

Confined Heat Treatment Prussian Blue Analogue for Enhanced Electrocatalytic Oxygen Evolution

Yanhua Zeng,‡ Gao-Feng Chen,‡ Zhouyang Jiang, Liang-Xin Ding, Suqing Wang and Haihui Wang**

School of Chemistry & Chemical Engineering, South China University of Technology, Guangzhou 510640, China

*The corresponding authors: lxding@scut.edu.cn; hhwang@scut.edu.cn

‡These authors contributed equally to this work

Experimental Section

Chemicals. Ni foam (NF) (1cm×2cm), obtained from Changde Liyuan Material Company (China). Nickel (II) nitrate hexahydrate [$Ni(NO_3)_2 \cdot 6H_2O$], Potassium hexacyanoferrate (II) trihydrate [$K4Fe^{II}(CN)_6 \cdot 3H_2O$], sodium citrate dihydrate ($C_6H_5Na_3O_7 \cdot 2H_2O$), hydrochloric acid (HCl), potassium hydroxide (KOH), and potassium chloride (KCl) were purchased from Sinopharm Chemical Reagent Company (China) and used without further purification. Nafion solution (5 wt%) and commercial RuO_2 catalyst from Sigma Aldrich Corp were applied and tested. Deionized (DI) water was used in all the experiments.

Preoxidation of Ni foam (NF). All pieces of Ni foam (1cm×2cm) were rinsed in acetone, 0.5 M HCl, and deionized (DI) water for 10 minutes sequentially. Then, transferred into round-bottom flask with 3 M HCl aqueous solution, soaked for 25 minutes at 90°C of oil bath. After that, taken out and cleaned with DI to remove the residual solution. Finally, in order to oxidize, the NFs were placed at room temperature in the laboratory environment for two days.

Preparation of $NiFe^{II}$-PBA on NFs. Two pieces of NF were immersed into 20 mL of 0.02 M Potassium hexacyanoferrate (II) trihydrate solution, containing 22.21 mg sodium citrate dehydrate. Then the solution was stilled for 18 h at room temperature. Finally, the pieces were washed with distilled water and dried at room temperature for one day.

Fabrication of $NiFe^{II}$-PBA-SE/NF catalyst electrode. The as-prepared $NiFe^{II}$-PBA in-situ grown on NF was immersed into 15 mL solution containing 7.0 g KCl, and then frozen and dried for 45 h. The dried pieces were put in a porcelain boat at the furnace for further calcination at 300, 350, 400, 450, 500, 800 °C for 1 h in flowing Ar atmosphere respectively, with the ramp rate of 1°C/min. After cooling down, the pieces were washed with distilled water, dried at the room temperature.

Fabrication of $NiFe^{II}$-PBA-NSE/NF-400 catalyst electrode. The as-prepared $NiFe^{II}$-PBA in-situ grown on NF were directly put in a porcelain boat at the furnace for further calcination at 400 °C for 1 h in flowing Ar atmosphere, with the ramp rate of 1 °C/min. After cooling down, the pieces were washed with distilled water, dried at the room temperature.

Preparation of $NiFe^{II}$-PBA powder. 20 mL of 0.02 M Potassium hexacyanoferrate (II) trihydrate solution, containing 22.21 mg sodium citrate dehydrate, as solution A. 20 mL of 0.02 M Nickel (II)

nitrate hexahydrate solution, as solution B. Then solution B was added into solution A, and the mixed solution was stilled for 18 h at room temperature. To obtain the powder of $NiFe^{II}$-PBA, the stilled solution was centrifuged with distilled water and ethanol, two times respectively. Then the powder was dried at 50 °C in a drying oven.

Surface Optimization of $NiFe^{II}$-PBA. The obtained powder was put into a porcelain boat at the furnace for further calcination at 300, 350, 400, 450, 500, 800 °C for 1 h in flowing Ar atmosphere, respectively, with the ramp rate of 1°C/min.

Materials characterization. The morphology and structure of the as-prepared samples was examined by using field-emission scanning electron microscopy (FESEM; JEOL, JSM-7000F) and transmission electron microscopy (TEM; JEOL, JEM-2100F). The crystallographic and composition of samples were characterized by using powder X-ray diffraction (XRD, Bruker, D8 ADVANCE) with Ka radiation (λ=1.5418 Å) and fourier transform infrared spectroscopy (FT-IR, Bruker, VERTEX 33). The X-ray photoelectron spectroscopy measurement was carried out on a monochromatic Al Kα radiation (XPS, Kratos Axis Ulra DLD) to analyze the element state and component of the samples.

Electrochemical tests. All electrochemical measurements were performed on a CHI 760D electrochemical workstation (Chenhua, shanghai, China) at room temperature with a three-electrode system, which connects with the modified NF as the working electrode, a platinum foil and a saturated calomel electrode as the counter electrode and the reference electrode in a 1 M aqueous KOH electrolyte, respectively. OER polarization curves were obtained by linear sweep voltammetry (LSV) at scan rate of 5 mV/s. Before OER measurements, the electrodes were electrochemically pretreated with repeating cyclic voltammetry (CV) for 12 scan cycles from 1.0 V to 1.6 V (vs. RHE) in 1.0 M KOH. Through the pretreat process, the oxygenated surface functional groups were increased and the hydrophilicity and wettability of the surface got further improved. Polarization curves were corrected for an ohmic drop (iR) tested by electrochemical impedance spectroscopy (EIS). And EIS was measured by AC impedance spectroscopy within the frequency range from 0.1 to 100 kHz in 1.0 M KOH. The long-term durability test was conducted without iR-correction at the potential of 1.6 V (vs. RHE), separately. All potentials were converted to reversible hydrogen

electrode (RHE), using equation $E_{RHE} = E_{SCE}+0.242\ V+0.0591\times pH$, where E_{RHE} is the potential referred to RHE, E_{SCE} is the tested potential against the reference electrode.

Preparation of catalyst electrode. 5.0 mg powder was dispersed in 1 mL ethanol, along with 10 μL Nafion solution (5 wt%). The mixture was sonicated for 30 min. Then 400 μL of prepared ink was dropped on the Ni foam at the catalyst loading of 2.0 mg/cm^2.

Tafel slope calculation.

$$\eta = b\ log|j| + a$$

where η is the overpotential, j is the current density, b is the Tafel slope, and a is the intercept relative to the exchange current density.[1]

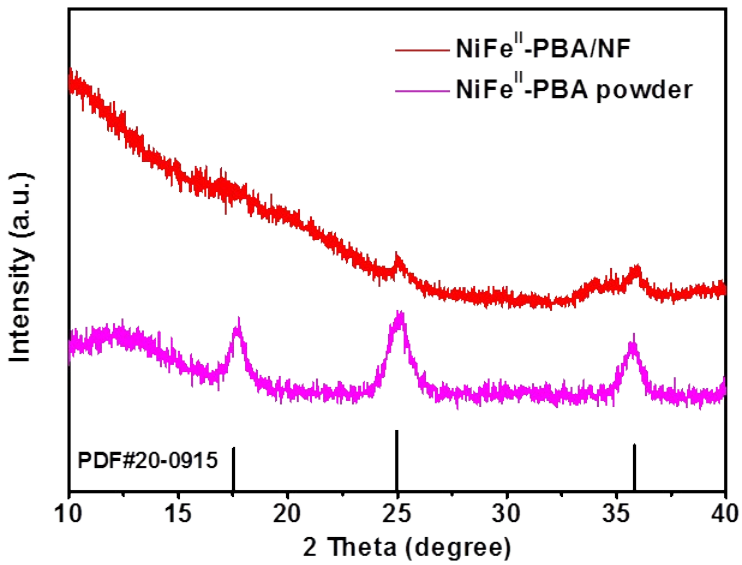

Fig. S1. XRD patterns of $K_2NiFe(CN)_6$ powder and $K_2NiFe(CN)_6$ *in-situ* grown on NF without heat-treatment.

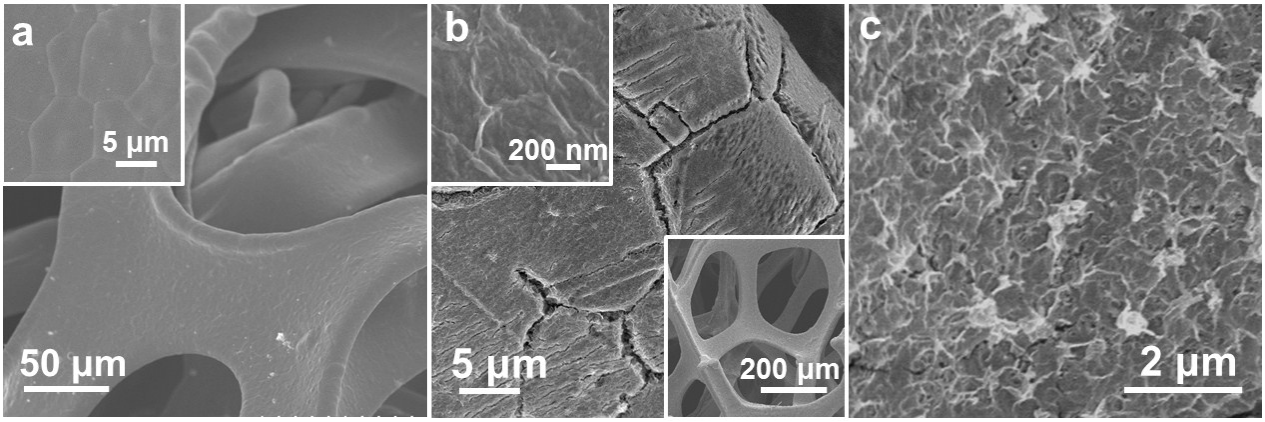

Fig. S2. SEM images of initial NF and preoxidized NF.

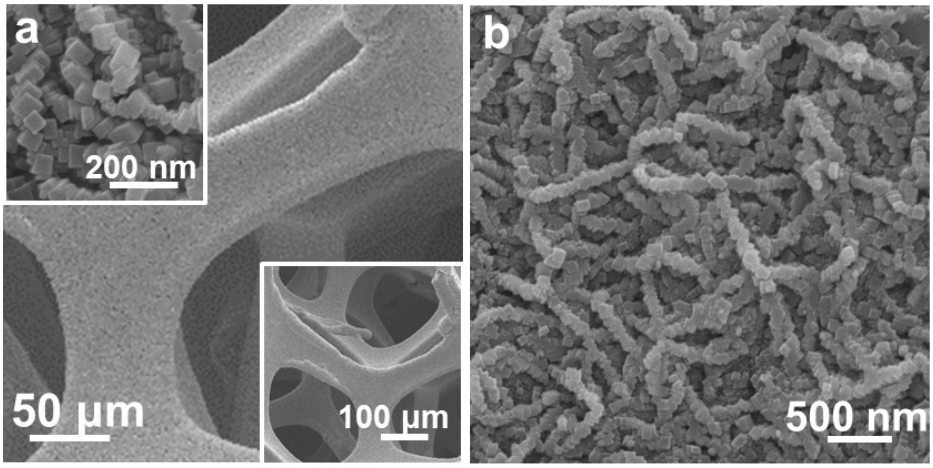

Fig. S3. a,b) SEM images of $NiFe^{II}$-PBA *in-situ* grown on NF.

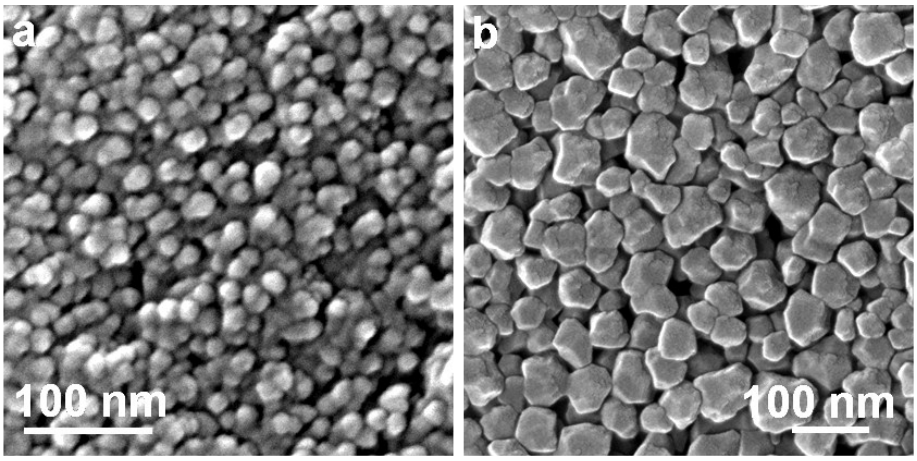

Fig. S4. a) SEM images of NiFeII-PBA and b) NiFeII-PBA-400 powder. The morphology of $NiFe^{II}$-PBA powder is similar to that of $NiFe^{II}$-PBA in-situ synthesis on nickel foam with a cubic-like structure, but with disordered distribution compared with a chain distribution of $NiFe^{II}$-PBA in-situ synthesis on nickel foam. Moreover, the SEM image of $NiFe^{II}$-PBA-400 powder shows that agglomerated particles are generated after heat treatment at 400 ^{o}C. It indicates that it is beneficial for synthesis of well-ordered $NiFe^{II}$-PBA by using the self-sacrifice of NF substrate as nickel source, and so that it would avoid agglomeration and get dispersible nanoparticles of $NiFe^{II}$-PBA-NSE/NF-400. Certainly, this agglomerated structure is one of factors that show a negative effect for the catalytic performance of the $NiFe^{II}$-PBA-400 powder.

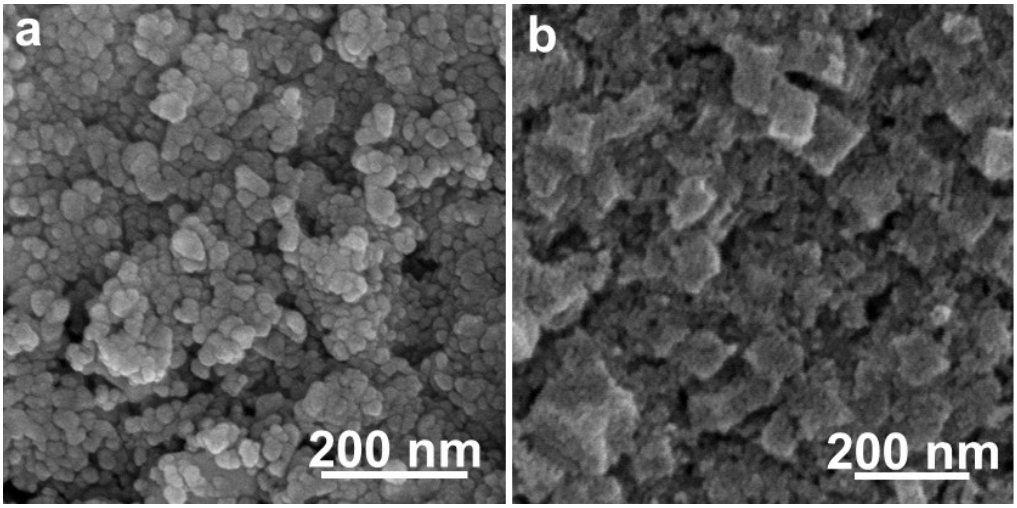

Fig. S5. SEM images of a) without encapsulation of salt during calcination, b) with salt encapsulation during calcination.

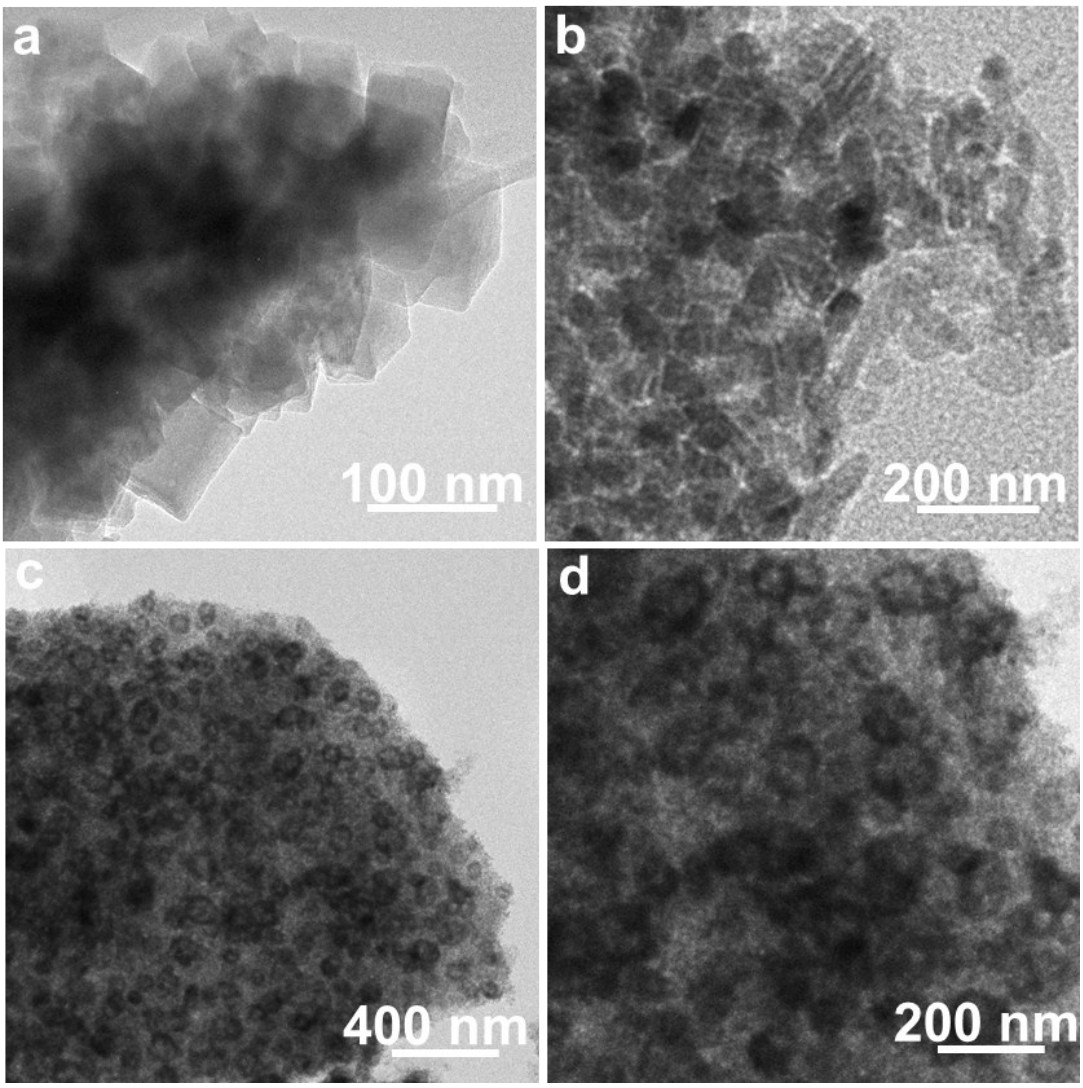

Fig. S6. HRTEM images of a) initial $NiFe^{II}$-PBA on NF without heat-treatment, b) $NiFe^{II}$-PBA-NSE/NF-400, c, d) $NiFe^{II}$-PBA-SE/NF-400.

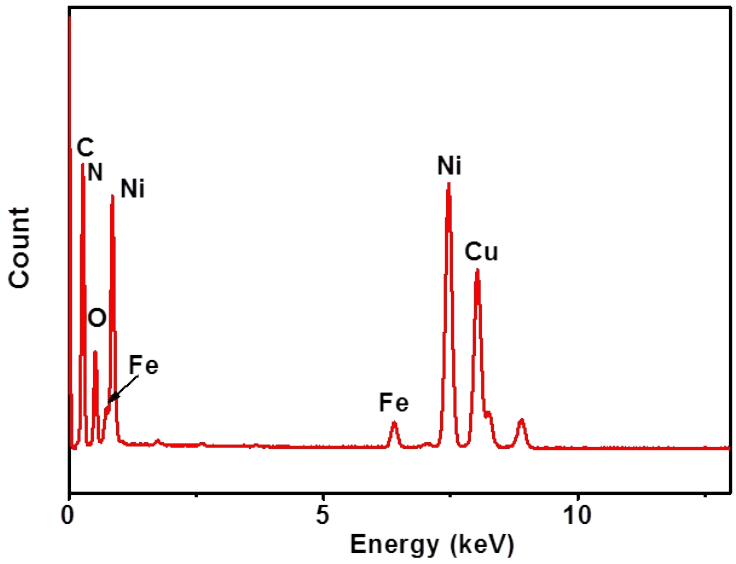

Fig. S7. EDS spectrum of $NiFe^{II}$-PBA-SE/NF-400.

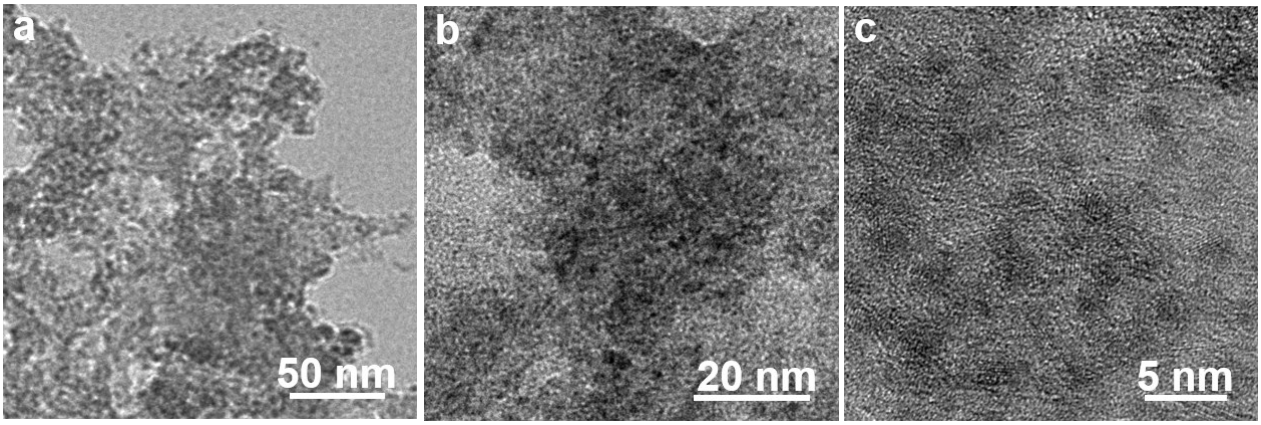

Fig. S8. HRTEM images of a, b, c) $NiFe^{II}$-PBA-SE/NF in 800 °C pyrolysis condition.

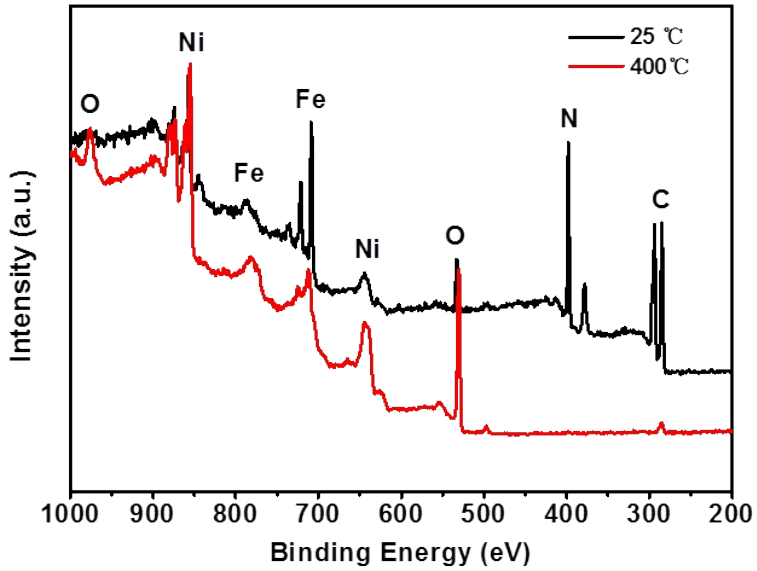

Fig. S9. XPS spectra of initial $NiFe^{II}$-PBA without heat-treatment and heat-treated at 400 °C.

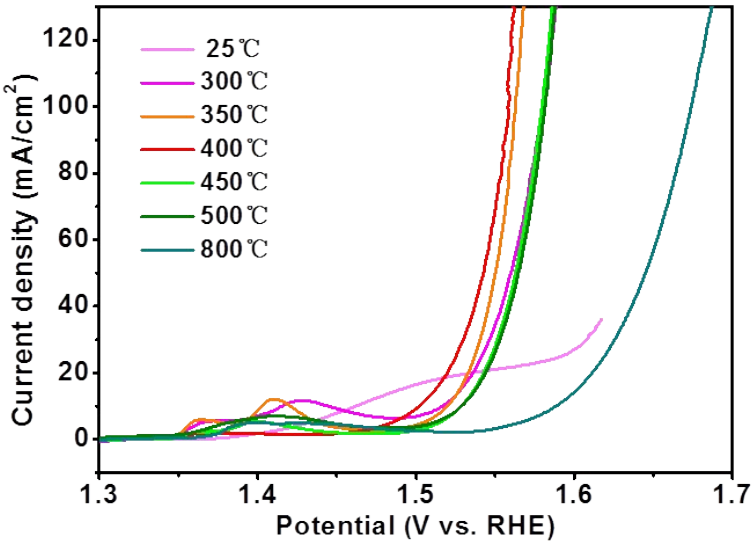

Fig. S10. IR-corrected linear sweep voltammetry (LSV) curves of initial $NiFe^{II}$-PBA powder and heat treated in different temperature from 300 °C to 800 °C in 1.0 M KOH at a scan rate of 5 mV/s.

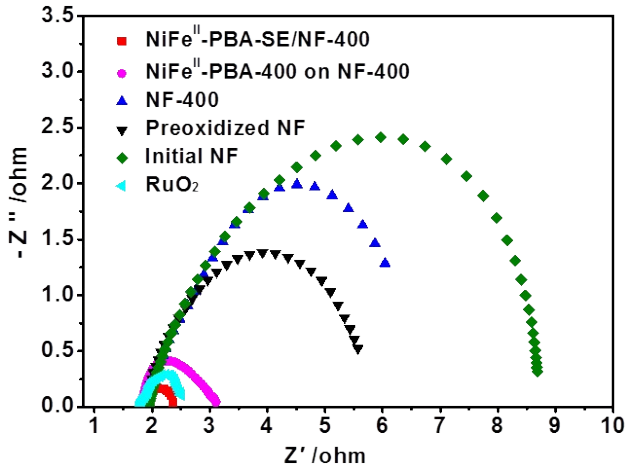

Fig. S11. Nyquist plots of NiFeII-PBA-SE/NF-400, NiFeII-PBA-400 powder on NF-400, NF-400, preoxidized NF, initial NF and RuO_2 with a potential of 1.6 V (vs. RHE). The R_{ct} of NF-400, preoxidized NF and initial NF are significantly larger than that of NiFe^{II}-PBA-SE/NF-400, NiFe^{II}-PBA-400 on NF-400 and RuO_2. This result illustrates that the support materials show little correlativity to the increasing conductivity (charge transfer rate) for NiFe^{II}-PBA-SE/NF-400 and the main contributor of conductivity is the PBA-derived materials.

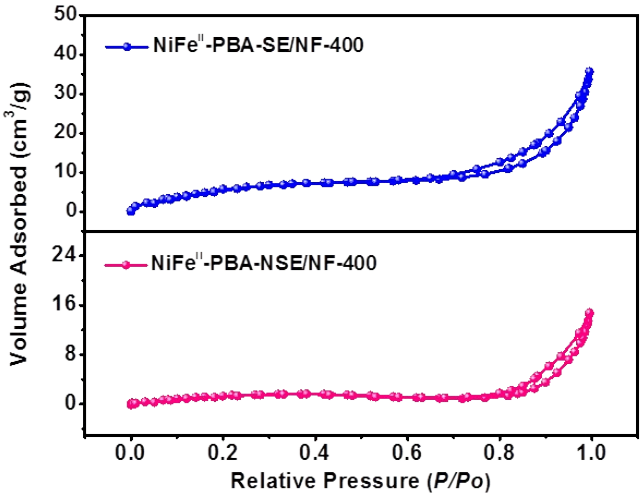

Fig. S12. Nitrogen adsorption-desorption isotherm of NiFe^{II}-PBA-SE/NF-400 and NiFe^{II}-PBA-NSE/NF-400. The specific surface area of NiFe^{II}-PBA-SE/NF-400 is up to 25.26 m^2/g, however that of NiFe^{II}-PBA-NSE/NF-400 is only 7.32 m^2/g. This testifies that the specific surface area of NiFe^{II}-PBA-SE/NF-400 gets increased, benefiting from the hollow structure formed with salt encapsulation.

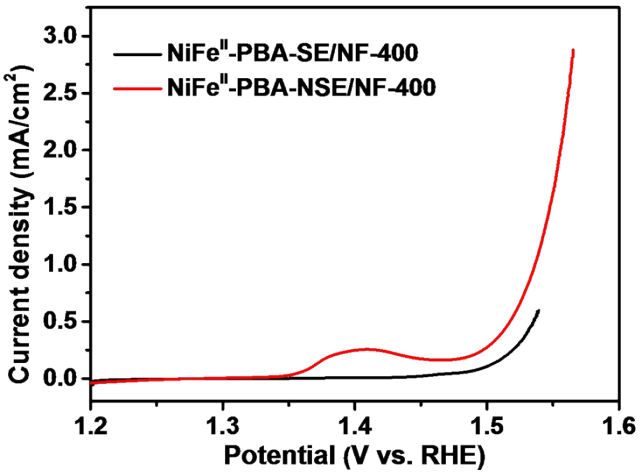

Fig. S13. IR-corrected linear sweep voltammetry (LSV) curves normalized to BET surface area. the current density of NiFe^{II}-PBA-SE/NF-400 (after normalized to BET surface area) is far lower than that of NiFe^{II}-PBA-NSE/NF-400 at same overpotential, in contradiction to the results after normalized to the geometric area. It further demonstrates the enhanced OER catalytic activity of the NiFe^{II}-PBA-SE/NF-400 should be mainly attributed to its larger active area.

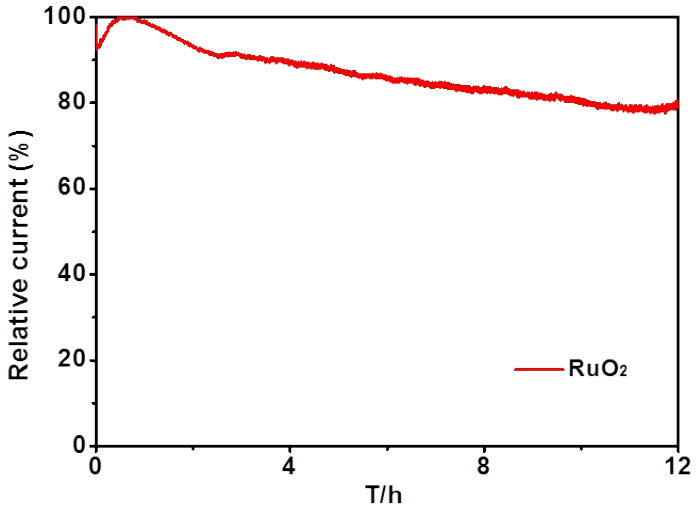

Fig. S14. Durability assessment of RuO_2 for OER at a constant potential of 1.6 V (vs. RHE). It shows that RuO_2 maintains 79.5% of its initial current after 12 h continuous test.

Table S1. A brief comparison of OER electrocatalysts derived from MOF and PBA reported recently.

Catalysts	J (mA/cm^2)	η (mV)	Tafel slope (mV/dec)	reference
$NiFe^{II}$-PBA-SE/NF-400	50	285	53.1	This work
	10	＜245		
Porous NiP	10	300	64	2
$Ni(OH)_2$ nanoplate	10	360	111	2
NiO nanoplate	10	430	81	2
Ni-Co mixed oxide cages	10	380	50	3
$NiFe^{II}$@NC	10	239	75	4
NF@NC-$CoFe_2O_4$/C NRAs	10	240	45	5
$CoSe_2$/CF	10	297	41	6
Porous Co_3O_4/C NAs	30	318	81	7
Ni_2P@C/G	10	285	44	8
Ni@NC-800	10	280	45	9
Co-NC/CNT-800	10	354	78	10
Co-Ni-Se/C/NF	30	275	63	11
Co-Fe-P-1.7	10	244	58	12
Co_3O_4@CoP	10	238	51.4	13

Table S2. A brief comparison of MOF directly as OER electrocatalysts reported recently.

Catalysts	J (mA/cm^2)	η (mV)	Tafel slope (mV/dec)	reference
MAF-X27-OH	10	292	-	14
$Co(TCNQ)_2/Co$	15	310	76	15
UTSA-16	10	408	77	16
Fe3-Co2@Ni	10	225(pH=13)	48	17
Fe:2D-Co-NS@Ni	10	211 (pH=13)	46	18

References

1 Y. Feng, H. Zhang, Y. Zhang, X. Li and Y. Wang, *ACS Appl. Mater. Interfaces*, 2015, **7**, 9203-9210.

2 X.-Y. Yu, Y. Feng, B. Guan, X. W. Lou and U. Paik, *Energy Environ. Sci.*, 2016, **9**, 1246-1250.

3 L. Han, X. Y. Yu and X. W. Lou, *Adv. Mater.*, 2016, **28**, 4601-4605.

4 L. Du, L. Luo, Z. Feng, M. Engelhard, X. Xie, B. Han, J. Sun, J. Zhang, G. Yin and C. Wang, *Nano Energy*, 2017, **39**, 245-252.

5 X. F. Lu, L. F. Gu, J. W. Wang, J. X. Wu, P. Q. Liao and G. R. Li, *Adv. Mater.*, 2017, **29**, 1604437.

6 C. Sun, Q. Dong, J. Yang, Z. Dai, J. Lin, P. Chen, W. Huang and X. Dong, *Nano Research*, 2016, **9**, 2234-2243.

7 C. Zhang, J. Xiao, X. Lv, L. Qian, S. Yuan, S. Wang and P. Lei, *J. Mater. Chem. A*, 2016, **4**, 16516-16523.

8 M. Wang, M. Lin, J. Li, L. Huang, Z. Zhuang, C. Lin, L. Zhou and L. Mai, *Chem. Commun.*, 2017, **53**, 8372-8375.

9 Y. Xu, W. Tu, B. Zhang, S. Yin, Y. Huang, M. Kraft and R. Xu, *Adv. Mater.*, 2017, **29**, 1605957.

10 F. Yang, P. Zhao, X. Hua, W. Luo, G. Cheng, W. Xing and S. Chen, *J. Mater. Chem. A*, 2016, **4**, 16057-16063.

11 F. Ming, H. Liang, H. Shi, X. Xu, G. Mei and Z. Wang, *J. Mater. Chem. A*, 2016, **4**, 15148-15155.

12 T. Zhang, J. Du, P. Xi and C. Xu, *ACS Appl. Mater. Interfaces*, 2016, **9**, 362-370.

13 J.Zhou, Y. Dou, A. Zhou, R.-M. Guo,M.-J. Zhao and J.-R. Li, *Adv. Energy Mater.*, 2017, **7**, 1602643.

14 X.-F. Lu, P.-Q. Liao, J.-W. Wang, J.-X. Wu, X.-W. Chen, C.-T. He, J.-P. Zhang, G.-R. Li and X.-M. Chen, J. Am. Chem. Soc, 2016, **138**, 8336-8339.

15 Y. Wei, X. Ren, H. Ma, X. Sun, Y. Zhang, X. Kuang, T. Yan, D. Wu and Q. Wei, *Chem. Eur. J.*, 2018, **24**, 2075-2079.

16 J. Jiang, L. Huang, X. Liu and L. Ai, *ACS Appl. Mater. Interfaces*, 2017, **9**, 7193-7201.

17 J.-Q. Shen, P.-Q. Liao, D.-D. Zhou, C.-T. He, J.-X. Wu, W.-X. Zhang, J.-P. Zhang and X.-M. Chen, *J. Am. Chem. Soc.*, 2017, **139**, 1778-1781.

18 J. Huang, Y. Li, R.-K. Huang, Dr.C.-T.He, Y.-T.Xu, X.-Y.Tian,Dr.S.-Y.Liu, Z.-M. Ye,F.Wang, Dr.D.-D. Zhou, Dr.W.-X. Zhang,Prof. J.-P. Zhang, *Angew. Chem. Int. Ed.*, 2018, **57**, 4632-4636.